Liquid Crystals
Publication details, including instructions for authors and subscription information:
http://www.informaworld.com/smpp/title~content=t713926090

Electroconvection in dimeric nematic liquid crystals with short-range smectic C order: dynamical characteristics

M. Petrov[a]; E. Keskinova[a]; B. Katranchev[a]; H. Naradikian[a]
[a] Institute of Solid State Physics, Bulgarian Academy of Sciences, Sofia, Bulgaria

Online publication date: 15 January 2011

To cite this Article Petrov, M. , Keskinova, E. , Katranchev, B. and Naradikian, H.(2011) 'Electroconvection in dimeric nematic liquid crystals with short-range smectic C order: dynamical characteristics', Liquid Crystals, 38: 1, 41 — 52
To link to this Article: DOI: 10.1080/02678292.2010.524944
URL: http://dx.doi.org/10.1080/02678292.2010.524944

Liquid Crystals,
Vol. 38, No. 1, January 2011, 41–52

Taylor & Francis
Taylor & Francis Group

Electroconvection in dimeric nematic liquid crystals with short-range smectic C order: dynamical characteristics

M. Petrov*, E. Keskinova, B. Katranchev and H. Naradikian

Institute of Solid State Physics, Bulgarian Academy of Sciences, Sofia, Bulgaria

(*Received 27 April 2010; final version received 15 September 2010*)

We describe the specific features of electroconvection (EC) in the nematic liquid crystal (NLC) phase with short-range smectic C order (the seventh homologue of the p,n-alkyloxybenzoic acid, 7OBA, which is dimeric). These features are revealed below a definite temperature (T^*) within this liquid crystal phase. By polarisation analysis of the azimuthal in-plane director deflection in the EC regime we suggest that this instability has a twist-type character. We indicate that the specificity of the temperature variation of the electroconductivity and the EC in 7OBA is determined by the smectic tilt angle magnitude and the dimer's compactness within the supramolecular complexes. We find that response times below T^* are about two times shorter than those in classical NLCs, as an equalisation of both response and decay times, which is preferable in LC display techniques. A fourth frequency harmonic is detected for the first time in the N state.

Keywords: liquid crystals; electroconvection; dimeric nematic

1. Introduction

The electroconvection (EC) in liquid crystals (LCs) has been intensively studied for more than three decades [1–9]. Under standard conditions, nematic (N) LCs of positive conductive ($\sigma_a = \sigma_\parallel - \sigma_\perp > 0$), negative dielectric ($\varepsilon_a = \varepsilon_\parallel - \varepsilon_\perp > 0$) ($\parallel$ and $\perp$ mean parallel and perpendicular to the N director $\boldsymbol{n}$) anisotropies and planar orientation (the director is along the x direction of the LC cell's xy plane), with the system in the presence of a d.c. or a.c. electric field, applied in the z direction, exhibit a forward bifurcation to normal rolls (NRs) pattern known as Williams domains. These domains usually occur as a primary instability, with wave vector $\boldsymbol{q}$ parallel to the equilibrium director orientation $\boldsymbol{n}_o \equiv x$ [4].

While the classical one-dimensional (1D) Carr–Helfrich (CH) theory [10, 11] describes well the NRs instability, this theory is not directly applicable for the description of the more complicated three-dimensional (3D) EC patterns, appearing as oblique rolls (ORs), zigzag rolls and other complex instabilities [3, 5, 9]. CH standard theory describes all ECs with $\varepsilon_a \leq 0$ including those of small positive value of ε_a [3].

Many papers have been published, mainly by the Bayreuth–Budapest LC groups [3, 8, 9,12–22], aiming to introduce more clarity into the boundless scope of combinations of the sign and magnitude of ε_a and σ_a, LC geometry (from planar to homeotropic), the diversity of LC materials from the classical calamitic N-(4-methoxybenzylidene)-4-butylaniline (MBBA) to the nowadays widely studied bent core LCs [23–27]. The ECs in achiral and chiral smectic C (S_C) LCs, although these instabilities were successfully studied long ago [28–31], nowadays have no adequate development. As one can see in [29, 31], a possible mechanism for EC in S_C LCs was the twist instability, induced by the azimuthal director fluctuation in xy cell plane. Nowadays such fluctuations and the corresponding twist instability are widely used for the EC interpretation in the case ($\varepsilon_a < 0$, $\sigma_a < 0$) of calamitic, as well as for bent-core, LC materials both in homeotropic and planar orientations. Details of the EC in S_C materials with temperature-independent and temperature-dependent tilt angles, as well as the competition of the EC and Freedericksz transitions, can be found in [31, 32].

The new stage of intensive electrohydrodynamical instability studies started with the work [5] where the classical 1D theory was expanded in order to embrace a more complex 3D EC description, known nowadays as standard theory. On this basis the EC, which is characterised by a diversity of pattern manifestations, was divided into two categories, standard and non-standard EC (sEC and nsEC, respectively). The standard EC was well described by the anisotropic CH mechanism. The corresponding mechanism, however, for the nonstandard EC is not determined yet. It could isotropic, or another mechanism still unknown.

We will present briefly the anisotropic CH mechanism (see the details in [3, 19]) and the isotropic mechanism [33–40]. The anisotropic mechanism is well described in the classical and contemporary EC

*Corresponding author. Email: mpetrov@issp.bas.bg

ISSN 0267-8292 print/ISSN 1366-5855 online

DOI: 10.1080/02678292.2010.524944
http://www.informaworld.com

presentations. The guiding publications are the above cited works [1–22] for the calamitic LCs and [23–27] for the bent-core LCs. In essence, the anisotropic EC mechanism is as follows: when an a.c. voltage $\sqrt{2}U\cos(\omega t)$ (where U is the effective amplitude and ω is the frequency) is applied on a liquid crystal cell (LCC) in the z direction, the conductivity anisotropy σ_a of the material in combination with small fluctuation modes of the director tilt lead to lateral charge separation in the x direction and a periodically modulated flow field. This flow field in turn couples to the director field thus inducing an EC in the form of convective rolls at a threshold field $E_{th} = U_{th}d$ (where d is the cell thickness). At E_{th} the stabilising elastic and dielectric torques on the director are outmatched by destabilising hydrodynamic torques. Under standard conditions a regular sequence of bright and dark stripes, viewed in an optical microscope, are seen. Thus the ultimate reason for the appearance of the EC pattern lies in the anisotropy of the electrical conductivity.

The EC in the LCs with relatively small electroconductivity anisotropy, however, is due to the inhomogeneous bulk charge distribution. Unlike in the anisotropic CH mechanism, the charge carriers pile up on one of the LCC electrodes due to unipolar injection from the other electrode. The destabilising hydrodynamic torque resulting from σ_a is now depressed and is not able to destabilise the torque equilibrium and cannot trigger the EC. This effect manifests at the moment when the decrease of the anisotropy is large enough to start isotropy. Now the threshold field is $E_{th}^2 \sim \pi^4\eta\sigma/\varepsilon^2$ (where η is the viscosity). While the anisotropic mechanism was decisively developed to capture various ε_a, σ_a combinations and geometries, the isotropic mechanism is still not adapted to the observed isotropic ECs. Nevertheless, many of the EC pattern formations seem to obey this mechanism, which was proposed long ago by the Russian LC group [33–40]. Some new interpretations of the prewavy instability [9, 19], appearing in the nematic liquid crystals characterising with very high electroconductivity (discovered long ago and known as wide domains) are examples of the complex character of the EC instability in LCs, since one can assume a few possible mechanisms for this EC. Until now, however, a justification of the working mechanism, not only for the prewavy but also for the most of the nsECs, has not existed.

Some experimental investigations concerning the measurement of the twist azimuthal angle in the xy plane and the trends of the threshold field on temperature and frequency could throw a new light on the complicated field of EC driving mechanisms. A convenient system in this sense is the N phase appearing beyond the S_C phase on cooling, which we will consider as being N with short-range S_C order [35]. We emphasise that the instability in the N phase with short-range smectic order is strongly influenced by the generation and frustration of the smectic layers inside the N phase. Thus the EC instability in these Ns is predetermined from that of the S_C phase and *vice versa*. Furthermore, the smectic order fluctuations in the Ns, where quasi-smectic supramolecular N complexes form (known in the literature as cybotactic groups – a classical designation), undoubtedly influence the character of the EC instability, and provoke inversion of the sign and magnitude of ε_a and σ_a as a result of the easy distribution of the charges in the layer's planes.

This inversion, however, manifests itself in two ways: just at the isotropic (I)–N phase transition temperature (as e.g. in 4,n, alkyloxyazoxybenzene, 7OAB), or inside the N phase (as e.g. in the seventh, eighth and ninth homologues of p,n-alkyloxybenzoic acid, 7,8,9OBA). Both these materials, due to the absence of a smectic A (S_A) phase in their phase diagrams, have the characteristic of having a S_C tilt angle ω, which is temperature independent.

Brand *et al.* [7] have studied two homologues of the substance 4'-hexyloxypheyl 4-decyloxybenzoate, which display N and S_A phases, and found that the inversion of the sign of σ_a, from positive to negative, keeping $\varepsilon_a < 0$, provokes two different patterns – NRs at high temperatures and a time-dependent two-dimensional (2D) localised pattern at low temperatures, where the CH mechanism is broken. A clear differentiation of the σ_a variation for a group of compounds (four homologues of the series 4-n-alkyloxy-phenyl-4-n'-alkyloxy-benzoates) displaying only N (marked as 5/8), N and S_C (marked as 8/7), N, S_A, S_C (marked as 10/4) and N, S_A, S_C, smectic B (10/6) was elaborated by Kochowska *et al.* [8] aiming to embrace a wide class of combinations of negative dielectric anisotropy ($\varepsilon_a < 0$) and σ_a ranging from positive to negative, with special emphasis on the ($\varepsilon_a < 0$, $\sigma_a < 0$) case at planar alignment.

Looking at the temperature dependence of the conductivity anisotropy σ_a presented in [8], one finds that the behaviour of the compound 8/7 is closed to that of 7OAB, while both 10/4 and 10/6 change σ_a sign inside the N phase. So the σ_a temperature variation of 10/4 and 10/6, although they display a S_A phase beyond the S_C phase to a great extent resembles that of 7,8OBA, by not displaying a S_A phase. The difference is, however, that σ_a in 7,8OBA changes only in magnitude and keeps its positive sign in the whole N temperature range. The EC instability below and above the temperature, where σ_a changes only its magnitude inside the N phase (we will mark this temperature as T^*), must be of special interest. This interest is quickened further since only 7,8,9OBA, in contrast to the other above-mentioned LC materials that also display N and S_C phases, are constituted from dimer molecules,

which change from closed dimers to open dimers and in turn to monomers when the temperature increases [41].

We will analyse the results of 7OBA (those for 8,9OBA will be presented in other work) following descriptions of sEC and nsEC the presented in the literature both in calamitic and bent-core LCs. Using both microtextural-polarisation analysis and the laser diffraction method at normal and oblique illumination, we will put into practice a real-time quantitative access to the electric field induced director field amplitude variations of the complex N system – Ns with short-range S_C order build by hydrogen bonds in dimer molecules. We will restrict our investigation to the low-temperature N range (below T^*), where the S_C order fluctuations dominate. Our purpose is also to estimate the director location for the in-plane fluctuations, causing the EC instability. The detection of the corresponding flow responsible for the observed EC patterns will also be attempted. Furthermore, analysing the threshold and polarisation characteristics of the patterns, their decay from EC to the ground non-excited state and the existence of Fourier modes with frequencies harmonic to the electric field frequency, we will test the possible EC mechanism of these LC materials.

2. Experimental results and discussion

2.1 The sample preparation

The experiments have been carried out on 4,n-heptyloxybenzoic acids (7OBA) with phase diagram: $Cr \overset{92^oC}{\longleftrightarrow} S_C \overset{98^oC}{\longleftrightarrow} N \overset{146^oC}{\longleftrightarrow} I$.

The substance was placed between two parallel glass plates whose surfaces express the xy plane and are coated with transparent electrodes, with indium tin oxide (ITO) unidirectionally rubbed in the x direction providing the initial director orientation $\boldsymbol{n}_o$. The cell thickness $d = 12$ μm between the glass plates was maintained with Mylar spacers.

The temperature of the sample was varied at a rate of 0.1°C min^{-1} by a hot stage temperature controller (Linkam TMS 90). An a.c. field $E = (0, 0, E_z)$ of frequency f was applied across the sample in the z direction. The EC optical texture, in the xy plane, was observed by use of a video camera (Hitachi) simultaneously with the diffraction process. Micropolarisation analysis of the patterns formed at the electric field parameter variations was carried out by a microscope (Zeiss NU2). In turn, the optical signal was studied by video capturing equipment.

The analysis of EC instability in 7OBA requires a description of the ε_a and σ_a temperature variation within the N phase, following that presented in the literature [42–45]. We have reproduced the values of these parameters at temperatures close to T^*, where σ_a reaches its maximum before decreasing with further cooling down to the S_C phase, as will be described below.

For 7OBA, ε_a varies between 0.03 and 0.011 corresponding to a temperature variation between 140 and 100°C [45]. The maximum value of ε_a is 0.04 at 122°C. Below this temperature, ε_a continuously falls (at 110°C it is 0.015) but this is due to the decrease of $\varepsilon_{||}$, since below 122°C $\varepsilon_\perp$ smoothly increases up to the nematic-smectic C transition temperature (T_{NC}), where the ε_a sign sharply changes from positive to negative, as a result of the sharp diminution of $\varepsilon_{||}$ just at the transition to the S_C phase. Thus $T^* = 122$°C determines the point where ε_a starts to fall. For fullness we note that above 140°C ε_a tends to zero.

The σ_a variation in the N temperature range of 7OBA is as follows: from 0.18×10^{-9} (Ω^{-1} cm^{-1}) at 140°C it increases to 0.7×10^{-9}(Ω^{-1} cm^{-1}) at 122°C, below which it falls to 0.21×10^{-9} (Ω^{-1} cm^{-1}) at 110°C (see also [44, 45]). Considering the electro-conductivity temperature variation in a more convenient presentation $\sigma_{||}/\sigma_\perp$ [42], one finds that from 1 at T_{NI} (the temperature of the N–I transition) it increases to 1.18 at $T^* = 122$°C and then falls to 1.01 (with approximate equalisation of the $\sigma_{||}$ and $\sigma_\perp$ values) near to T_{NC}, but keeps the same sign ($\sigma_a > 0$).

We emphasise that similar electric behaviour occurs in 8OBA, which has $\sigma_a > 0$, like 7OBA while in 9OBA $\sigma_a < 0$ in the entire N region. This could be assigned to the longer molecule of 9OBA, providing easy realisation of compact (coordination of the monomers, closed and open dimer fluctuations in space and time with a trend to generate a quasi-smectic layer) smectic-like supramolecular complexes, still below T_{NI}. It is evident that such compactness is more natural in 7OAB, where the LC constituting molecules are only monomers.

This peculiarity has not been considered until now, in spite of the acceptance in the literature that the sign inversion of σ_a within the N phase appearing beyond the S_A or S_C phases at cooling [8] or just below T_{NI} reveals a decrease of $\sigma_{||}$, with respect to $\sigma_\perp$, due to the more easy charge distribution within the grown smectic layer. This effect is synonymously indicated in the S_A phase [46], while in the S_C phase it depends also on the tilt angle ω, as the sign of σ_a could be positive if $\omega \geq \pi/4$ or negative if $\omega < \pi/4$. This was indicated by Rondelez [42], considering both the dimeric N phase of 8OBA and the monomeric N phase of 7OAB. He assumed that inside the supramolecular complex the conductance normal to the growth smectic planes (σ_n) is smaller than that inside the planes (σ_p) and simplified an otherwise complicated situation in the complexes by accepting the diffusion constant of the

charge carriers to be much smaller than $\xi^2(T)/\tau$, where $\xi(T) \approx 400$ Å is the correlation length and τ is the life time of the supramolecular cluster. In this limit $\sigma_\parallel$ and $\sigma_\perp$ of the N system may be obtain simply by averaging the local conductivity tensor over all allowed orientations of the supramolecular clusters. On this basis ω was calculated and measured by X-ray diffaction [47] and that in 7OAB was found to be ≈34°, while in 8OBA and 7OBA it was found to be 55° and 50° respectively (larger than the limit for the sign inversion $\pi/4$).

Thus we can categorise the 7OBA investigated here as the EC case where ε_a is positive and small, and σ_a is also positive, but undergoes an anomaly at $T^* \approx$ 122°C. As we will see below, at this temperature, similarly to substances where the σ_a sign inverses [8], the EC noticeably changes its basic electro-optical characteristics. Therefore, the anomaly in the magnitude of σ_a is revealed as a decrease of $\sigma_\parallel$ and a compensating increase of $\sigma_\perp$, due to the easier distribution of charges in the growing smectic layers. The distribution effectiveness, however, depends on the S_C tilt angle magnitude.

A sketch of the experimental set-up of the diffraction is indicated in [48]. We used a low-power He–Ne laser (≈1 mW) of wavelength $\lambda_L = 650$ nm. A photodiode or 2D camera at a distance l of approximately 600 mm from the LC cell was used for the far-field diffraction analysis. The photodiode aperture was 3 mm × 3mm.

In order to study the relaxation of the EC patterns the intensity of the diffracted light was monitored. The photodiode was positioned at the centre of the selected fringe. Its output was fed into a converter, and a recording of the intensity at an adequate rate was made. We subtracted the 'parasitic' intensity after switching off the field, ensuring the room to be dark enough.

The linear polarised light of the laser used was tuned to follow the direction of the easy axis $\boldsymbol{n}_o$.

2.2 Characterisation of the EC patterns

We concentrated on the EC instability below the characteristic temperature $T^* = 122$°C at 12 μm for the substance 7OBA studied here, aiming to analyse this instability in the N region where the EC exists in the large quasi-smectic supramolecular clusters, where σ_a starts to inverse its magnitude but retain its sign due to the larger value of the tilt angle inside the supramolecular complexes. At the same time, ε_a is positive but small as the average value in the region $(T^* - T_{NC})$ is $\varepsilon_a \approx 0.013$ [43, 45].

We applied an a.c. sinusoidal voltage U to the planar aligned LC cell. The driving parameters are the voltage, which for convenience in some cases will be transformed into dimensionless form by normalisation to the EC onset (threshold) voltage U_{th}, $\epsilon = (U^2 - U_{th}^2)/U_{th}^2$, the frequency f of the applied electric field and the temperature T.

We will describe the EC pattern evolution for three typical temperatures (120, 110 and 105°C) starting from T^* (122°C) where the inversion of the σ_a magnitude sets in. We will describe the EC pattern formation first for 80 Hz where the diffraction dynamical analysis was done.

At a temperature of 120°C, stripe domains (rolls), forming an angle ±45° with respect to $\boldsymbol{n}_o \equiv x$, start at a threshold voltage of 6.9 V. At a second threshold (7.55 V) the stripe domains, after fluctuations normal to the roll's axes, transform to wavy forms (Figure 1), and then coalesce in a regular square pattern. They are well observed when the polariser is at 18° with respect to $\boldsymbol{n}_o \equiv x$. The EC threshold versus frequency for a temperature of 120°C and a thickness of 12 μm is indicated in Figure 2.

A competition between the Freedericksz transition and EC instability threshold exists in such materials with very small ε_a (for details see [32]). Our measurements indicate that the Freedericksz transition appears slightly above the EC threshold and manifests itself as a strong colouring typical for the dielectric reorientation. For example, at 120°C and 1.5 kHz the EC threshold is 12.8 V and the Freedericksz transition appears at 14 V, while at 2 kHz we observe only the Freedericksz transition. Frequencies above 2 kHz stop the charge carrier mobility and pure dielectric (Freedericksz) reorientation sets in.

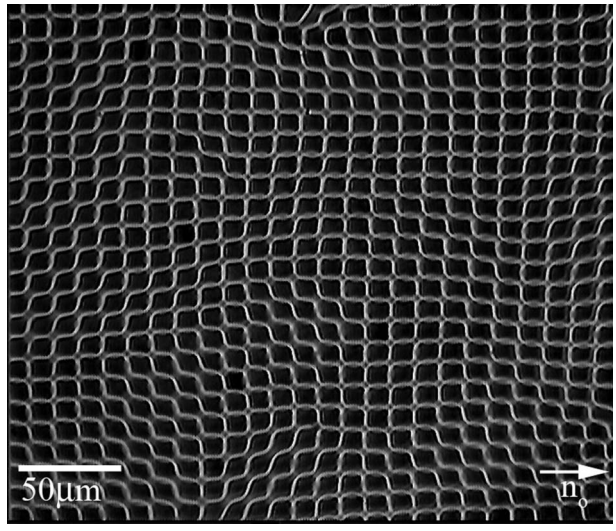

Figure 1. 2D EC texture of 7OBA (the transformed in rolls in wavy forms) at $U_{th} = 7.55$ V, $T = 120$°C, $d = 12$ μm.

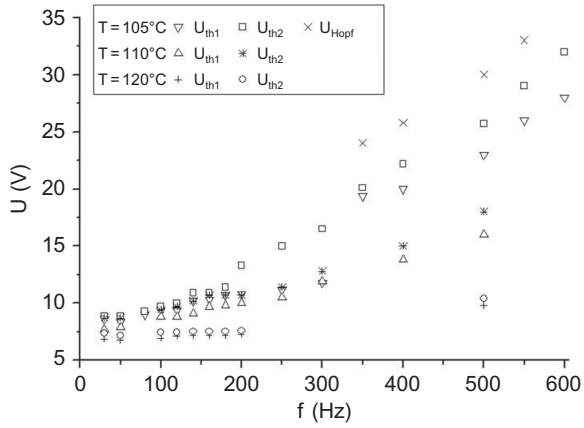

Figure 2. The EC threshold versus frequency for temperatures of 120°C, 110°C, 105°C, where $d = 12$ μm.

The EC at 110°C and 80 Hz at $U_{th1} = 9.1$ V appears directly as a 2D pattern. Here two EC thresholds also exist, which are very discernable above 500 Hz (see Figure 2). At the second threshold, the 2D cell-like domains after fluctuating along two directions, forming angles ±45° with the x axis, transform into elongated cells with long axis perpendicular to the easy direction (Figure 3). In this case one can see pure dielectric reorientation at frequencies above 3 kHz and for voltages higher than 68 V.

At 105°C both ε_a and σ_a reach very low values (as we described above) near to the isotropic ones, but keep their positive signs. This is why the EC below this temperature is unique, as regards to EC in classical Ns. At 80 Hz a 2D EC texture appears at the

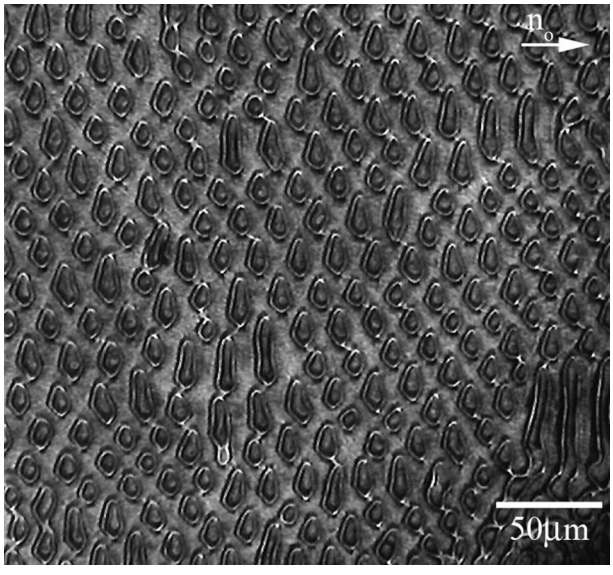

Figure 3. Transformation of the domains in elongated 'cells' with the long axis perpendicular to the easy direction at a temperature of 110°C, a frequency of 1 kHz and $U_{th} = 38$ V.

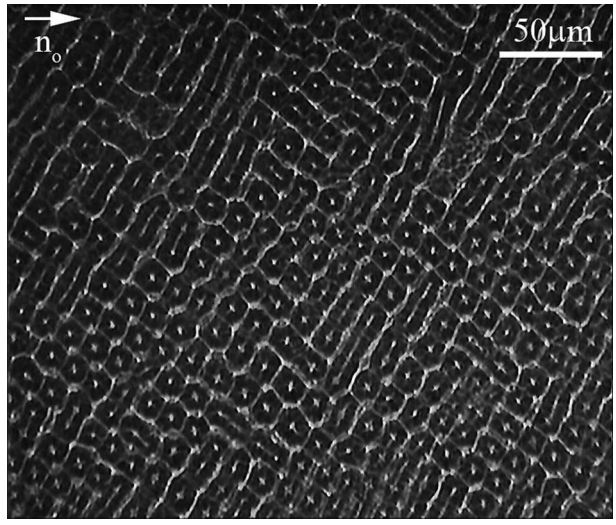

Figure 4. A 2D EC texture appears at the threshold U_{th1} as a primary instability at a temperature of 105°C, a frequency of 80 Hz and a voltage of 10 V.

threshold U_{th1} as a primary instability (Figure 4). It is revealed by cell-like domains arrayed in two directions including the angle 45° with the x direction. The second 2D EC texture (arising as elongated cells with long axis perpendicular to the easy direction (Figure 4)) determines U_{th2} which is a few volts above U_{th1} (see Figure 2).

Above 500 Hz, there are three voltage thresholds. At the second threshold U_{th2} (27 V), the cell-like domains already formed at U_{th1} transform into stationary space localised domains, which with a further voltage increase above U_{th3} (32 V) start to move

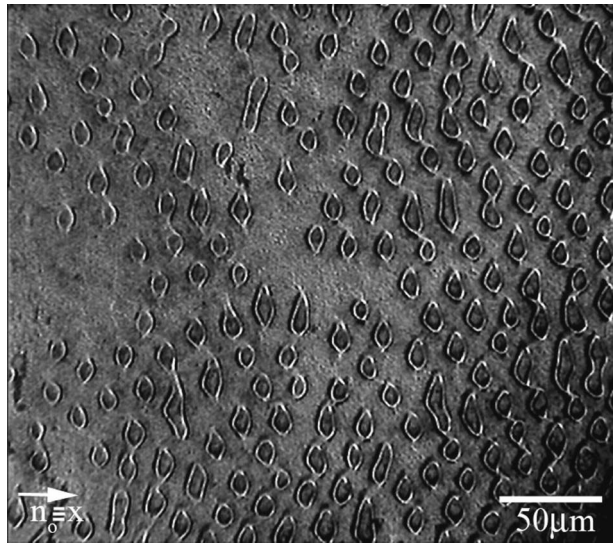

Figure 5. The texture represents domains located moving perpendicular to $\boldsymbol{n}_o$ at a frequency of 500 Hz (32 V) and a temperature of 105°C.

perpendicular to the x direction – the domains are localised in space and in time (Figure 5). Thus U_{th3} presents the onset of travelling domains, interpreted in the literature as Hopf bifurcation [49], characteristic of the consideration of the LC system as a weak electrolyte. At 1 kHz, however, only the second threshold texture (51 V) is seen as a stationary located domain coexisting with the surrounding non-convective state (the localised domains emerge at the same places) and the travelling domains set in at $U_{\text{th3}} = 60$ V. The pure Freedericksz transition can be seen above 3.5 kHz.

2.3 Dynamical characteristics of EC: relaxation times of the director

We initiated the pattern decay by a momentary switching off (of 15 μs) of the applied voltage. Both the decay and response times have been scanned, extracted and measured by recording the odd and even diffraction intensities $I_{\pm 1}$ and $I_{\pm 2}$ at normal or oblique illumination, respectively [50, 51]. The oblique illumination is more effective in respect to putting into practice real-time access to the director amplitude in EC onset. This can be done since the EC patterns reveal a spatial director modulation. This modulation produces an optical phase grating with a constant that of the EC wavelength $\Lambda = 2\pi/q$.

The relaxation time and especially the decay time are important parameters, which reveal the LC system dynamics since the EC patterns allow us to keep track of the pattern relaxation by means of the fringe intensity decay during the system transition to the equilibrium ground state [18, 20]. The electrical parameters, driving the EC, fall off at the time of the decay process, and only the pattern wavelength, the elastic and viscous material constants works after the switch off of the electric field. Therefore, the decay time measurement allows us to actually assess the material parameters.

The response and the decay times are measured from 10–90% amplitude modulation as a function of the applied voltage. The angle of oblique illumination α varies between $\pm 10°$ and $\pm 30°$. In Figure 6, we indicate a representative picture of the response (pattern growth) and decay times. On and off mean the switch on and the switch off of the electric field. The plateau of the trend expresses the established EC regime, where the ***n*** modulation occurs. In fact the modulation of the director field imprints important processes on the diffraction pattern, which provides a fast and quantitative access to the dynamics of the dominant Fourier mode of the director pattern by corresponding analysis and allows the harmonic frequencies to be extracted.

Looking at the corresponding picture of the response and decay times for EC at 130°C

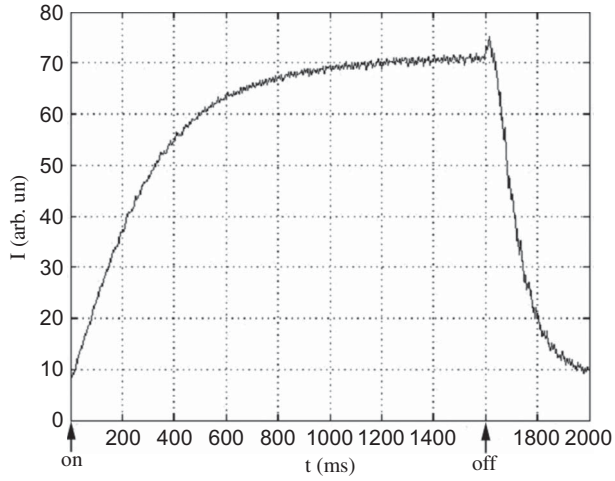

Figure 6. A representative picture of the response (pattern growth) and decay times. On and off mean the switching on and the switching off of the electric field. The plateau of the trend expresses the established EC regime, where the ***n*** modulation occurs, $T = 105°$C.

characterising this instability in the temperature region $T^* < T < T_{\text{NI}}$, where a classical N behaviour of the LC system is expected, we found that the initial light scattering level (scattering background) below T^*, where enough large clusters are formed, is an order higher than the scattering level above this temperature. The scattering intensity after switching off of the field in this case relaxes from 70 at the plateau to about 10 (in arbitrary units) at the off state (equal to the on state), i.e. the background makes about 14% of the complete signal intensity. For 130°C, however, the scattering intensity from 60 falls close to zero, meaning that the background below T^* only reflects a slight parasitic intensity (the room darkness was ensured during the diffraction registration). The larger (one order) background scattering intensity of the laser light below T^* detects the quasi-smectic cluster sizes, which are comparable with the laser wavelength.

Increasing the voltage above the threshold, we indicate in Figure 7 the decay curves obtained when applying different $\epsilon = (U^2 - U_{\text{th}}{}^2)/U_{\text{th}}{}^2$ values. The curve $\epsilon = 0.96$ in the figure indicates that the deformation of the director in the EC regime is already large enough comparatively with those at $0.6 < \epsilon < 0.8$. Such deformations are revealed by an increase of the intensity (peak) at the starting point of the decay at $\epsilon = 0.96$.

Furthermore, we found for the first time that the structural transition at T^* changes the director modulation characteristics of the EC instability, as well as the nonlinearity of the system, thus leading to the

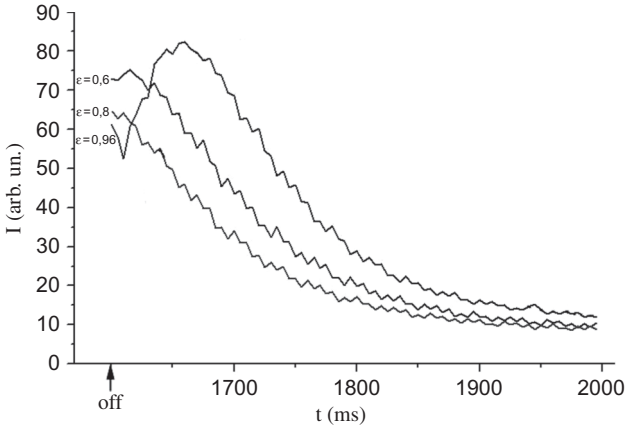

Figure 7. The decay curves obtained when different $\epsilon = (U^2 - U_{th}^2)/U_{th}^2$ values were applied (U_{th} = 15 V at a temperature of 105°C). The curve $\epsilon = 0.96$ indicates the largest ***n*** deformation and reveals a slight increase of the intensity (peak) at the starting point of the decay.

induction of a fourth harmonic of the excited a.c. electric field ($4f$), coexisting with the second harmonic $2f$. The harmonic $2f$ in the EC instability was discovered long ago and is typical only for classical Ns (without smectic order fluctuations) like MBBA [4]. The amplitudes of the $2f$ and $4f$ harmonics vary with field, as they increase at first with increasing electric field and after a maximal value at $\epsilon \approx 7$ decrease. There is a difference between the harmonic amplitudes for normal ($\alpha = 0$) and oblique (e.g. $\alpha = 30°$) illuminations, as the latter are larger at the same value of the electric field, indicating the advantage of the oblique illumination for realisation of real-time access to the director field amplitude in the EC regime. Furthermore, at oblique illumination, the harmonic registration for both harmonics starts just at the threshold, while for the normal illumination the registration starts at higher voltages. The ratio of the harmonic amplitudes $2f/4f$ at a fixed electric field value is $\approx$15 for $\epsilon \approx 7$ and oblique illumination, and 30 for normal illumination.

3. Discussion

We consider in the present work the EC for $\varepsilon_a > 0$, $\sigma_a > 0$, which have small magnitudes. In general (see [33–40]) EC for the category ($\varepsilon_a > 0$, $\sigma_a > 0$) is divided into two cases: (i) NRs are first observed when the field is increased for $0 < \varepsilon_a < 1/3\varepsilon_{a1}$, where $\varepsilon_{a1} = \varepsilon_{||}\sigma_a/\sigma_{||}$, and then this is followed by dynamic scattering; (ii) at $1/3\,\varepsilon_{a1} < \varepsilon_a < \varepsilon_{a1}$ only NRs are observed, since before achieving turbulence director reorientation takes place. In particular, for the classical NLCs (e.g. MBBA) with $\sigma_{||}/\sigma_{\perp} = 1.3$, which is constant within the N temperature range, case (i) is realised at $\varepsilon_a \leq 0.1$ and case (ii) at $0.1 < \varepsilon_a < \varepsilon_{a1}$ [33]. Thus the EC complexity increases due to the enormous combinations of the electrical anisotropies, material constants, LC cell geometry and smectic order fluctuations.

Taking into account the fact that the compounds 10/4 and 10/6 [8] display a S_A phase beyond the S_C phase and σ_a inverses its magnitude inside the N phase, one can conclude that, although 7OBA does not display a S_A phase in its phase diagram, in this material the generation of the locally layered structures in the quasi-smectic complexes starts as being S_A-like at the point T^*. On further cooling, however, a tilt angle (ω) in the layer forms which transforms into the S_C phase for $\omega \approx 50°$. At special boundary conditions we have indicated this effect [52, 53], and found an induction of the S_A phase, as an intermediate one, between the N and S_C phases. The EC in the 7OBA system to a great extent resembles the EC described in [8] and at the same time exhibits some details not observed and analysed until now.

Now we will present the microtextural polarisation analysis undertaken to test the director field behaviour in the presence of a driving electric field.

The best contrast for the primary EC in the pattern at 120, 110 and 105°C was achieved when the polariser and analyser were not just crossed at $\pi/2$ but were at an angle of 18° for the temperatures 120°C and 110°C and 28° for the temperature 105°C. These patterns were also visible under nearly parallel polarisers with reduced contrast. With one polariser, an analysis typical for the shadowgraph method, the patterns at all temperatures were slightly visible. This suggests that the director had periodic modulations in the xy plane, exhibiting azimuthal twist modulation, so as to be able to describe the EC in the S_C phase [28–31] and recently considered to be an explanation of the abnormal EC patterns of parallel stripes, square and other patterns both in calamitic [8, 9, 19] and bent-core [23–27] LCs.

The microtextural polarisation analysis gives us the possibility to estimate the amplitude of the azimuthal ***n*** modulation φ_o at varying over-threshold voltages or frequencies by rotation of the sample between crossed polarisers.

For the N phase of 7OBA we have indicated, by the known crystal rotation method [54], that the polar angle (between the cell's normal and ***n***) is 80.6° below T^*, while above this temperature it is $\approx$90° (normal planar anchoring). This result indicates that the director below T^* is tilted with respect to the xy plane at an angle θ (the ***n*** projection on this plane is $c = n\cos\theta$). This ***n*** location below T^* presumes a homogeneous tilt out of the xz plane (a tilt plane perpendicular to the cell plane), as occurs in the case when a previously splay Freedericksz transition forms such an angle at a large enough positive ε_a and $\sigma_a < 0$ [19].

If the director was chosen to be in the polariser direction, before EC, then in the EC regime the bright

regions express a rotation of the polarisation plane of the light deviation by the ***n*** projection, while the dark regions express the fact that this projection rests close to this plane. So the twist out of the tilt plane inverses the dark and bright domain lines, and the polarisation direction. Practically, this is a result of the Mauguin adiabatic low – the light is guided by the twist [24, 25]. This is the basis of twist spatial modulation of the director (spatial variation of the effective refractive index). Therefore, the increase of ***n*** deflections due to voltage, frequency or temperature actions, provides twist bulk deformations. As a result, the LC system, in order to minimise the distortion energy, undergoes a modulated structure.

In order to measure the voltage and frequency dependence of the ***n*** twist modulation, we rotated the sample under crossed polarisers. Before starting the rotation ***n*** was located along the polariser's direction. We rotated the cell first in a clockwise direction until the intensity of the bright domains in the texture became minimised, indicating that ***n*** in these regions was actually located along the polariser's direction. Since in the opposite direction of rotation the intensity inverts, it follows that symmetric *n* modulation with respect to the $\boldsymbol{n}_o \equiv$ x initial orientation occurs.

The values of the azimuthal angle $\varphi(U)$ at 80 Hz for temperatures just below T^* (120°C) and for temperatures near to T_{NC} (105°C) are presented in Table 1. Note, however, that for the first temperature 120°C, at least for the voltages below 9 V (3 V above the threshold), the dependence $\varphi(U)$ resembles that indicated in [23] for the bent-core LC called CIPbis10BB in the ECs marked as PW2 (low frequency) and PW1 (high frequency), where PW means prewavy instability. They fit (considering the ECs as twist instabilities) the azimuthal ***n*** modulation for voltages slightly above the threshold with $\varphi(U) = \varphi_o[(U^2 - U_{th}{}^2)/U_{th}{}^2]^{1/2}$. A different trend occurs for $\varphi(U)$ for the same frequency at 105°C where φ decreases. Above 10 V the pattern is still stationary, but with a tendency to be space localised. φ does not depend on f for 105°C as well as for 120°C.

Considering the threshold behaviour of the EC below T^* we turn to the test of the possible driving destabilising mechanism operating in our material. The measured azimuthal angle variation indicates a periodic twist fluctuation (periodic going out of ***n*** from the vertical xz plane) and this is expected to be initiated by the coupling of the charge spreading out into the xy plane and the director field, thus resulting in a flow field $\mathbf{v} = (v_x, v_y, v_z)$, which is actually a 3D phenomenon, raising again the complexity of the problem. As a result, the process of the closing of the rolls in square or hexagonal localised states could be due namely to such in-plane director c rotation and the corresponding flow in the xy plane, which acts simultaneously with that in the xz plane. Therefore, the combination of such a complicated director ***n*** distortion at $U \geq U_{th}$ and the possibility of the electric charges moving more easily in the quasi-smectic layer planes leads to a resultant charge distribution and a correspondingly more complicated flow. This complicated distortion, charge distribution and flow, not taken into account by standard theory, could be visualised by the motion of dust particles. Using this method we found a motion of such particles, with circular trajectory. One observes that the particles periodically come into focus or out of focus, which manifests a vertical transference and a resultant moving of the particles on complex trajectories. At onset of the motion of the localised EC structures perpendicular (Hopf bifurcation) to $\boldsymbol{n}_o \equiv x$, we did not find the visualisation of the particle motion. This complicated distortion and charge distribution leads to an EC mechanism which is not coordinated with the well developed standard EC model.

Regarding the frequency threshold behaviour of the EC, one finds a difference between the curves for temperatures above T^*, where the standard EC over a large frequency range (expressed by NRs) develops, and that at temperatures below T^*, where three thresholds are indicated (Figure 2). As seen from the figure, U_{th} increases almost linearly with the frequency, like in the case of Ns with short-range smectic order, where σ_a is inversed from positive to negative, as related by the authors in [8, 21] to non-standard EC.

As is well known, Hopf bifurcation (indicating the travelling of localised domains) was predicted by the weak electrolyte model, as an extension of the 3D standard model [5]. We indicated in Figure 2 the onset of Hopf bifurcation, where it is considered as a threshold value revealed by the travelling stripes, and found that it increases linearly with frequencies higher than 400 Hz, meaning that below this frequency and

Table 1. The values of azimuthal angle $\varphi(U)$ at a frequency of 80 Hz for the temperature just below T^* (120°C) and for $T = 105$°C.

U, V	6,7	7,2	7,7	8,2	8,6	9,1	9,6	10,1	10,6	11,1	11,6	12,1	12,6
φ (105°C), °	–	–	–	–	7	13	13	12	11	10	8	7	8
φ (120°C), °	12	25	29	27	20	16	–	–	–	–	–	–	–

corresponding threshold voltage the diffusion, recombination and dissociation of charge carriers typical for the weak electrolyte mode could be decisive. So, at higher voltages and at higher frequencies, a fast charge acceleration ensures these processes occur. Here it is important that Hopf bifurcation appears at a lower temperature (105°C) and a very high voltage is needed for onset of the travelling.

The patterns we have observed remain stable above the threshold over an unusually wide voltage range, giving us the possibility to learn more about the EC, and especially the ***n*** deflection and corresponding optical modulation, by diffraction, across a broad scope. Presumably, when the Hopf bifurcation occurs accompanied with travelling localised domains, the diffracted light intensity cannot by scanned in order to get both dynamical parameters – relaxation times and harmonics. In all other over-threshold EC patterns, however, we succeeded in estimating these parameters by diffraction at normal and oblique incidences. In contrast to the assumptions for 8/7 in [8, 21] that is also characterised with a S_C phase below the N phase, we cannot state that the observed ECs resemble a dielectric regime which is typical for sEC. The last idea [22] for the role of the flexoelectricity is new, and may clarify some problems concerning the explanation of most of the peculiarities observed in the EC development of the N phase with S_C ordering studied here. Furthermore, for the frequency dependence of U_{th} a linearity remains while the temperature is changed, as the slope of the curves decrease with increasing temperature. It is interesting, however, that U_{th} decreases (for 80 Hz) almost linearly as the temperature T^*(122°C) is approached from below. For the bent-core Ns in parallel stripe EC the authors in [23] found a linearity of $U_{th}(T)$ when the clearing point was approached and the assumption was made that this regime is driven by an isotropic mechanism instead of an anisotropic one, where U_{th} diverges at the N–I phase transition temperature.

We found for 7OBA that $U_{th}(T)$ follows the σ_a variation between T^* and T_{NC}. When decreasing both σ_a and ε_a to very small values, a reciprocal increase of the threshold voltage was indicated near to T_{NC}, meaning that the isotropic nsEC mechanism could work below this temperature. In any case, however, we can state that near the S_C phase the isotropic mechanism and nsEC can be assumed, while in the temperature above T^* the anisotropic CH mechanism in the category of very small $\varepsilon_a > 0$ and $\sigma_a > 0$ can work. The Hopf bifurcation found, however, suggests that this type of EC bifurcation may be due to the decreased conductance $\sigma_{||}$ in the region below 110°C, which is consistent with the predictions of the weak electrolyte model [49].

We emphasise that most NLC materials appear to have negative Leslie coefficient α_3 [4], which leads to a stable orientation of the director in a constant shear flow. The substances, however, above a smectic–N transition, including 7OBA [55], exhibit positive α_3, providing a continuous rotation of ***n*** in a constant shear flow. Thus a periodic flow field, coupled to a twist angle modulation, could be the basis for the EC patterns observed below T^*.

The distribution of the observed 2D far-field diffraction field intensity that we observed from the 2D domain picture (Figure 4) expresses 2D director modulation, which is ***n*** azimuthal deflection and can be presented as $\varphi(x,y) \sim \varphi_o \cos(q_x x + q_y y)$, where q_x and q_y are the periodicities of the EC pattern. Such 2D φ fluctuations must indicate flow acting in the xy plane simultaneously with the normal flow in the xz plane. The normal flow [8] is characteristic of the modulation along x (NRs), which is $\theta(x,z) = \theta_o \cos q_x x \cos \pi z/d$, as θ is the director deflection in the xz plane.

Normally, for the initiation of such twist EC instability in the xy plane with azimuth φ one assumes that, since the twist constant K_{22} is significantly lower compared to the K_{33} bend elastic constant, the LC system undergoes twist deformations when ***n*** is deflected in an external field. Moreover when S_C or quasi-S_C layers are formed, the minimisation of the free energy occurs by director rotation on a cone around the layer's normal [4], thus also favouring twist fluctuations. As a result, the strip rolls tilted 45° with respect to $\boldsymbol{n}_o$ (formed due to the director tilt near to the surface) after fluctuation normal to their long axes transform into wavy stripes (see Figure 1), which in turn form a 2D square pattern. All these patterns are provided from the circular charge flow in the xy plane, which we have indicated by dust particles.

The laser diffraction at an oblique incidence indicated that using this incidence we can precisely control the decay process even at the onset of the EC instability [18, 20, 50, 51]. As indicated in Figure 7 the decay of the EC pattern is exponential. At larger amplitudes of the director we leave the linear regime and both amplitude and phase grating effects of the ***n*** modulation are important. On the other hand, by oblique incidence we can detect the very small director deflections near the threshold and in such a way increase the scope of the deflection angle values, as was indicated in [56]. In such a way, we increase the possibility of coordinating the controlled switching period of time with the higher over-threshold driving voltage (where some defects due to diffusion could confuse the pure growth of the deflection amplitude), and in turn of keeping the sharpness of the fringe as well as improving the precision of the response and decay time measurements.

Our measurements of the response and the decay times showed that in general the response times in the region above T^* are two times larger than those below this temperature, while the decay times are about twice as short. The ratio, however, of the response and decay times below T^* is on an order smaller than that above this temperature, where classical N behaviour was detected. This ratio is $\approx$1 below T^*, meaning equalisation of both response and decay times.

The shorter response times below T^* one can refer to as being caused by easier spreading of the charge carriers in the layers formed below this temperature inside the supramolecular clusters. This process combined with energetically favourable twist fluctuations provides faster EC pattern formation.

As was indicated, spatial harmonics appear mainly as a result of the nonlinear relation between the optical transmission profile and the ***n*** deflection profile [24, 27, 50, 51]. Using pure sine wave excitation at low frequencies, the response of the director field is symmetric, and the time dependent amplitude of ***n*** deflection preserves its sign and is symmetric in the two halves of the field period ($\varphi(t) = \varphi(t) + T/2$). As a consequence of these symmetries, the Fourier transform of $\varphi(t)$ contains only even multiples of the excitation frequency $f_o = 1/T$ (see [57]). Thus the system response is periodic in T, leading the lowest frequency in the dynamics of the system variables to be f_o. Practically, higher order spatial harmonics also must exist since they reflect the optical nonlinearity of the texture, but the diffraction experiment can detect only the low order ones, which are stronger.

We found two very visible harmonics $2f$ and $4f$ as a result of 2D Fourier transformation of the pattern. Therefore, slightly above the threshold, the diffracted light intensity is modulated with twice the frequency ($2f$) of the applied voltage. For higher over-threshold voltages the order of $4f$ appears. Hence, the $2f$ and in addition $4f$ modulation below T^* reveals the smectic layer formation and the in-plane (xy) azimuthal fluctuations $\phi(x,y)$, providing a superposition of two waves propagating with wave vectors q_x and q_y and amplitude ϕ_o, thus expressing the 2D EC pattern. The $4f$ harmonic presents higher order ***n*** oscillations, which is a new effect in NLCs.

On the basis of the time-dependent director fluctuation amplitude $\phi_o(t)$, the intensity of light diffracted by the EC domains could be expressed as a Fourier expansion $I(m,t) = I_o + A_{2f}\cos 2\omega t + A_{4f}\cos 4\omega t + \cdots$, where m is the diffraction order and A_{2f} and A_{4f} are the voltage-dependent coefficients. Practically, this series expansion ensures the Fourier transformation, where the harmonics are included.

4. Conclusion

We have described the special features of the EC instability in the dimeric N phase with short-range S_C order of the seventh homologue of p,n-alkyloxybenzoic acid. These features are due to the temperature anomaly of the electroconductivity anisotropy at a definite temperature (T^*) inside this phase. The anomaly has a maximum at T^* and causes a consequent decrease of the magnitude of the electroconductivity below this temperature, while its sign remains positive. Since the anisotropy of the dielectric constant is also small and positive, we assigned the EC in this LC material to category $\varepsilon_a > 0$, $\sigma_a > 0$, but with specific pattern, threshold and dynamical characteristics.

We found that in contrast to the N phase beyond the S_A phase at cooling or beyond the S_C phase with small tilt angles (less than 45°) where the electroconductivity in the layer is slightly larger than that normal to the layer leading to the inversion of the sign when the quasi-smectic complexes are large enough, in the material 7OBA studied here the magnitude of the anisotropy in the conductivity cannot fall below zero. This feature is due to the larger tilt angle (50°) in 7OBA and the disturbance of the compactness at the layer formation caused by the hydrogen bond conformation at the temperature variation, thus revealing the unique character of the EC in this material.

The very small values of both of the electric anisotropies near to the temperature of the N–S_C transition and the large quasi-smectic supramolecular clusters modifies the mechanism of the EC in this region, which seems to be non-standard and possibly isotropic. We have indicated that Hopf EC bifurcation (travelling domains) occurs in this region, which was not observed in the region near to or above T^*.

By polarisation analysis of the azimuthal in-plane (x,y) director deflection in the EC regime which is dependent on the temperature and the frequency, we have suggested a twist-type character of this instability, which is still not embraced by the contemporary 3D standard model, although this twist instability was discovered long ago for the S_C phase. In addition, we have stated that the twist EC instability is favoured in this material by the initial tilt of the director at the cell's boundaries in the low-temperature N state in combination with the easier charge distribution in the quasi-layers typical for this temperature range. We have also stated that the minimisation of the free energy in the S_C supramolecular complexes is realised by a rotation of the director on a cone, around the layer's normal. This rotation decisively favours the twist fluctuations.

We found that the appearance of the diffraction image at very small deviation from normal incidence allows a direct quantitative determination of the amplitudes of the director field very close to the threshold as well as in the broad over-threshold region. This gave the possibility of having a wide spectrum of data, concerning the threshold, pattern and dynamical characteristics to be deduced.

The measured shorter response times below T^* we referred to as being caused by easier spreading of the charge carriers in the layers formed below this temperature inside the supramolecular clusters. This process, combined with energetically favourable twist fluctuations, provides faster EC pattern formation, which in addition to the equalisation of both response and decay times is preferable in LC display techniques. In this sense the Ns below T^* could be of interest.

A fourth frequency harmonic, which is rather weaker than the second one, was detected for the first time in the N state. The harmonic's amplitude variation with increase of the electric field presumably displays the complex nonlinear response of the director field deflection and therefore merits special study.

We have indicated a larger (one order of magnitude in arbitrary units) scattering background below T^* in comparison with that above this temperature and related this effect to the generated supramolecular quasi-smectic clusters comparable in size with the laser light wavelength.

References

[1] Kramer, L.; Pesch, W. *Annu. Rev. Fluid Mech.* **1995**, *27*, 515–539.

[2] Kai, S.; Zimmerman, W. *Prog. Theor. Phys., Supl.* **1989**, *99*, 458–492.

[3] Kramer, L.; Pesch, W. In *Pattern Formation in Liquid Crystals*: Buka, A., Kramer, L., Eds.; Springer: New York, 1996.

[4] de Gennes, P.G.; Prost, J. *The Physics of Liquid Crystals*, 2nd ed.; Oxford University Press: New York, 1993.

[5] Bodenschatz, E.; Zimmermann, W.; Kramer, L. *J. Phys. (France)* **1988**, *49*, 1875–1899.

[6] Zhou, S.; Eber, N.; Buka, A.; Pesch, W.; Ahlers, G. *Phys. Rev. E: Stat., Nonlinear, Soft Matter Phys.* **2006**, 046211.

[7] Brand, H.; Fradin, C.; Finn, P.; Pesch, W.; Cladis, P. *Phys. Lett.* **1997**, *235*, 508–514.

[8] Kochowska, E.; Nemeth, S.; Pelzl, G.; Buka, A. *Phys. Rev. E: Stat., Nonlinear, Soft Matter Phys.* **2004**, *70*, 011711.

[9] Buka, A.; Eber, N.; Pesch, W.; Kramer, L. *Phys. Rep.* **2007**, *448*, 115–132.

[10] Carr, E.F. *Phys. Rev. A.* **1975**, *12*, 327–329.

[11] Helfrich, W. *J. Chem. Phys.* **1969**, *51*, 4092–4105.

[12] Richter, H.; Buka, A.; Rehberg, I. *Mol. Cryst. Liq. Cryst.***1994**, *251*, 181–189.

[13] Plaut, E.; Decker, W.; Rossberg, A.; Kramer, L.; Pesch, W.; Beladi, A.; Ribotta, R. *Phys. Rev. Lett.* **1997**, *79*, 2367–2370.

[14] Rossberg, A.; Eber, N.; Buka, A.; Kramer, L. *Phys. Rev. E: Stat., Nonlinear, Soft Matter Phys.* **2000**, *61*, R25–R28.

[15] Buka, A.; Dressel, B.; Otowski, W.; Camara, K.; Toth-Katona, T.; Kramer, L.; Lindau, J.; Pelzl, G.; Pesch, W. *Phys. Rev. E: Stat., Nonlinear, Soft Matter Phys.* **2002**, *66*, 051713.

[16] Dressel, B.; Pesch, W. *Phys. Rev. E: Stat., Nonlinear, Soft Matter Phys.* **2003**, *67,* 031707.

[17] Komineas, S.; Zhao, H.; Kramer, L. *Phys. Rev. E: Stat., Nonlinear, Soft Matter Phys.* **2003**, *67*, 031701.

[18] Eber, N.; Rozanski, S.A.; Nemeth, S.; Buka, A.; Pesch, W.; Kramer, L. *Phys. Rev. E: Stat., Nonlinear, Soft Matter Phys.* **2004**, *70*, 061706.

[19] Buka, A.; Eber, N.; Pesch, W. Connective patterns in liquid crystals, 2005. Electronic-Liquid Crystal Communications. http://www.e-lc.org/index.html (accessed Jul 12, 2005).

[20] Pesch, W.; Kramer, L.; Eber, N.; Buka, A. *Phys. Rev. E: Stat., Nonlinear, Soft Matter Phys.* **2006**, *73*, 061705.

[21] Toth-Katona, T.; Cauquil-Vergnes, A.; Eber, N.; Buka, A. *Phys. Rev. E: Stat., Nonlinear, Soft Matter Phys.* **2007**, *75*, 066210.

[22] Krekov, A.; Pesch, W.; Eber, N.; Toth-Katona, T.; Buka, A. *Phys. Rev. E: Stat., Nonlinear, Soft Matter Phys.* **2008**, *77*, 021705.

[23] Wiant, D.; Gleeson, J.T.; Eber, N.; Fodor-Csorba, K.; Jakli, A.; Toth-Katona, T. *Phys. Rev. E: Stat., Nonlinear, Soft Matter Phys.* **2005**, *72*, 041712.

[24] Stannarius, R.; Heuer, J. *Eur. Phys. J. E* **2007**, *24*, 27–33.

[25] Tamba, M.-G.; Weissflog, W.; Eremin, A.; Heuer, J.; Stannarius, R. *Eur. Phys. J. E* **2007**, *22*, 85–95.

[26] Kumar, P.; Hiermath, U.S.; Yelamaggad, C.V.; Rossberg, A.G.; Krishnamurthy, K.S. *J. Phys. Chem. B* **2008**, *112*, 9753–9760.

[27] Heuer, J.; Stannarius, R.; Tamba, M.G.; Weissflog, W. *Phys. Rev. E: Stat., Nonlinear, Soft Matter Phys.* **2008**, *77*, 056206.

[28] Goscianski, M.; Leger, L. *J. Phys. (Paris) Colloq.* **1975**, *36,* CI-231.

[29] Goscianski, M. *Philips Res. Rep.* **1975**, *30*, 37–55.

[30] Petroff, B.; Petrov, M.; Simova, P.; Angelov, A. *Ann. Phys. (Paris)* **1978**, *3*, 331–338.

[31] Petrov, M.P.; Petrov, A.G.; Pelzl, G. *Liq. Cryst.* **1992**, *11*, 865–886.

[32] Simova, P.; Petrov, M. *J. Phys. D: Appl. Phys.* **1981**, *14*, 1–8.

[33] Barnik, M.; Blinov, L.; Grebenkin, M.; Pikin, S.A.; Chigrinov, V. *Zh. Eksp. Theor. Fiz.* **1975**, *69*, 1080–1088.

[34] Barnik, M.; Blinov, L.; Grebenkin, M.; Trufanov, A. *Mol. Cryst. Liq. Cryst.* **1976**, *37*, 47–56.

[35] Blinov, L.; Barnik, M.; Lazareva, V.; Trufanov, A. *J. Phys. (Paris), Colloq.* **1979**, *40*, c3-263–268.

[36] Trufanov, A.; Blinov, L.; Barnik, M. *Zh. Eksp. Theor. Fiz.* **1980**, *78*, 622; Trufanov, A.; Blinov, L.; Barnik, M. *Sov. Phys. JETP* **1980,** *51,* 314–318.

[37] Pikin, S.; Chigrinov, V. *Sov. Phys. JETP* **1980**, *51*, 123–124.

[38] Blinov, L.; Chigrinov, V. *Electrooptic Effects in Liquid Crystal Materials*; Springer: New York, 1996.

[39] Rjumtsev, E.I.; Polushin, S.G. *Liq. Cryst.* **1993**, *13*, 623–628.

[40] Pikin, S.A. *Structural Transformations in Liquid Crystals;* Gordon and Breach: New York, 1991.
[41] Deloche, B.; Cabane, B. *Mol. Cryst. Liq. Cryst.* **1971**, *19*, 25–61.
[42] Rondelez, F. *Solid State Comm*. **1972**, *11*, 1675–1678.
[43] Kresse, H.; Lucke, K.H.; Schmidt, P.; Demus, D. *Wiss. Zeitschr. Univ. Halle* **1977**, *XXVI' M*, 147.
[44] Cuvatov, Z.; Capustin, A.; Trofimov, A. *Pisma, JETP* **1974**, *19*, 89–91.
[45] Cuvatov, Z.; Capustin, A.; Trofimov, A. *Tezisi Docl. Ivanovski Ped. Inst, Ivanovo* **1976**, *80*, 74–80.
[46] Carr, E.F. *Phys. Rev. Lett.* **1970**, *24*, 807–809.
[47] de Vries, A. *Mol. Cryst. Liq. Cryst.* **1970**, *10*, 31–37.
[48] Petrov, M.; Keskinova, E.; Katranchev, B. *J. Mol. Liq.* **2008**, *138*, 130–138.
[49] Trieber, M.; Kramer, L. *Mol. Cryst. Liq. Cryst. Technol Sect. A* **1995**, *261*, 311–326.
[50] Zenginoglou, H.M.; Kosmopoulos, J.A. *Appl. Opt.* **1989**, *28,* 3516; Zenginoglou, H.M.; Kosmopoulos, J.A. *J. Opt. Soc. Am. A* **1989,** *18*, 573–576.
[51] John, T.; Behn, U.; Stannarius, R. *Eur. Phys. J. B* **2003**, *35*, 267–278.
[52] Ivanov, N.B.; Petrov, M.P. *Liq. Cryst.* **1992**, *6*, 953–956.
[53] Ivanov, N.B.; Petrov, M.P. *Mol. Cryst. Liq. Cryst.* **1995**, *265*, 457–462.
[54] Shefer, T.J.; Nehring, J. *J. Appl. Phys.* **1976**, *48*, 1783–1792.
[55] Kneppe, H.; Schneide, F.; Sharma, N.K. *J. Chem. Phys.* **1981**, *77*, 3203–3208.
[56] Petrov, M.; Keskinova, E.; Naradikian, H.; Katranchev, B. *J. Optoelectron. Adv. Mater.* **2009**, *11*, 1226–1229.
[57] John, T.; Heuer, J.; Stannarius, R. *Phys. Rev. E: Stat., Nonlinear, Soft Matter Phys.* **2008**, *71*, 056307.